Effects of refractive index on glories

Philip Laven

9 Russells Crescent, Horley, Surrey RH6 7DJ, UK

*(philip@philiplaven.com)

Received 24 April 2008; revised 8 August 2008; accepted 14 August 2008;
posted 18 August 2008 (Doc. ID 95435); published 23 September 2008

Atmospheric glories are caused by backscattering of sunlight from spherical droplets of water (e.g., from fog or clouds). But what would glories look like if they were caused by scattering from more exotic substances, such as clouds of ethane as found on Titan? Examining backscattering as a function of the refractive index n of spherical droplets leads to the surprising conclusion that a glory's appearance is almost independent of n (at least for $1.03 < n < 1.7$)—unlike the colors of rainbows, which are critically dependent on the variation of n across the visible spectrum.

OCIS codes: 010.1290, 010.1350, 240.6690, 350.1260.

1. Introduction

Backscattering of sunlight from spherical droplets of water (e.g., from fog or clouds) can generate glories, which consist of a series of concentric colored rings centered on the antisolar point (corresponding to scattering angle $\theta = 180°$). At this very early stage of our exploration of the solar system, it is understandable that glories have not yet been observed on other planets or moons. Nevertheless, atmospheric optical phenomena have been detected on other planets: for example, in 1974, Hansen and Hovenier [1] analyzed earlier measurements of the polarization of sunlight reflected by Venus and, by detecting rainbow scattering, were able to deduce the size of the spherical droplets and their refractive index as a function of wavelength. The latter information strongly suggested that the droplets were formed of sulfuric acid—this hypothesis has subsequently been proved to be correct. Furthermore, halos on Mars and Venus have been reported by Können [2]. As a terrestrial glory has also been observed from space [3], it seems plausible that space probes will detect glories in atmospheres other than the Earth's, thus providing potentially valuable information about the nature of atmospheric particles.

0003-6935/08/34H133-10$15.00/0

Some atmospheres contain clouds of substances much more exotic than water: for example, clouds of ethane are known to exist on Titan [4]. To simulate the appearance of glories caused by ethane droplets, we would need information about the spectrum of sunlight, the Sun's apparent diameter, the size of the droplets (including the distribution of sizes), and the refractive index n of the droplets as a function of wavelength at the relevant temperature. This paper concentrates on how the appearance of the glory depends on the refractive index n.

Glories caused by scattering from water droplets have been successfully simulated in full color by using Mie theory calculations [3,5–7]. Comparison of such simulations with images of actual glories [3] indicates that most terrestrial atmospheric glories are caused by scattering of light from water droplets of radius r between 5 and 20 μm. Throughout this paper, the scattering calculations and simulations will be based on a value of $r = 10\,\mu$m. All the graphs and simulations in this paper have been generated by using the MiePlot computer program developed by the author. This program can be downloaded free of charge from http://www.philiplaven.com/mieplot.htm.

2. Mie and Debye Series Calculations

Figure 1 shows the results of Mie calculations for scattering of red light (650 nm) from a spherical droplet of radius $r = 10\,\mu$m for various values of n, assuming that the droplet is in a medium with

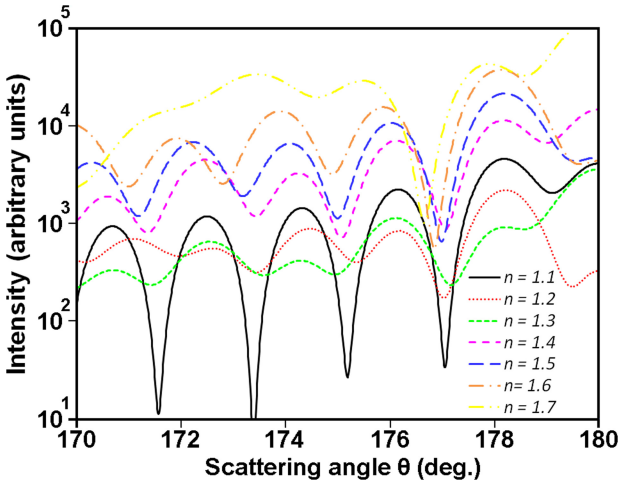

Fig. 1. (Color online) Mie theory calculations for scattering of red light ($\lambda = 650\,\text{nm}$) by a sphere of radius $r = 10\,\mu\text{m}$ as a function of scattering angle θ for various values of refractive index n of the sphere.

refractive index $n_{\text{med}} = 1$. Although the curves show significant differences, the maxima seem to cluster around specific values of scattering angle θ, such as at $\theta \approx 178°$, $\theta \approx 176°$ and $\theta \approx 174°$. To guard against the possibility that this apparent clustering might be caused by the particular values of n selected in Fig. 1, it is necessary to examine the scattered intensity as a function of θ and as a function of refractive index n of the scattering sphere—as in the false-color maps shown in Fig. 2(a). The colors in Fig. 2(a) represent the intensity of the scattered light as indicated by the false-color scale at the top right: zones of high intensity are shown as white, red, and yellow, while zones of very low intensity are shown as magenta and black. Note that the three panels of Fig. 2(a) show results for different polarization characteristics: the panel on the left is for polarization perpendicular to the scattering plane, the center panel is for polarization parallel to the scattering plane, and the panel on the right shows unpolarized light (i.e., the average of the other two panels).

For $n < 1.7$, the green and blue zones in Fig. 2(a) seem to be aligned horizontally around $\theta \approx 178°$, $\theta \approx 176°$, $\theta \approx 174.1°$, and $\theta \approx 172.2°$, while being clearly separated by magenta and black zones (indicating lower intensity). The horizontal green and blue zones in Fig. 2(a) correspond to the rings of the glory (in this case, a red glory, since the illumination is a monochromatic source of red light). The fact that

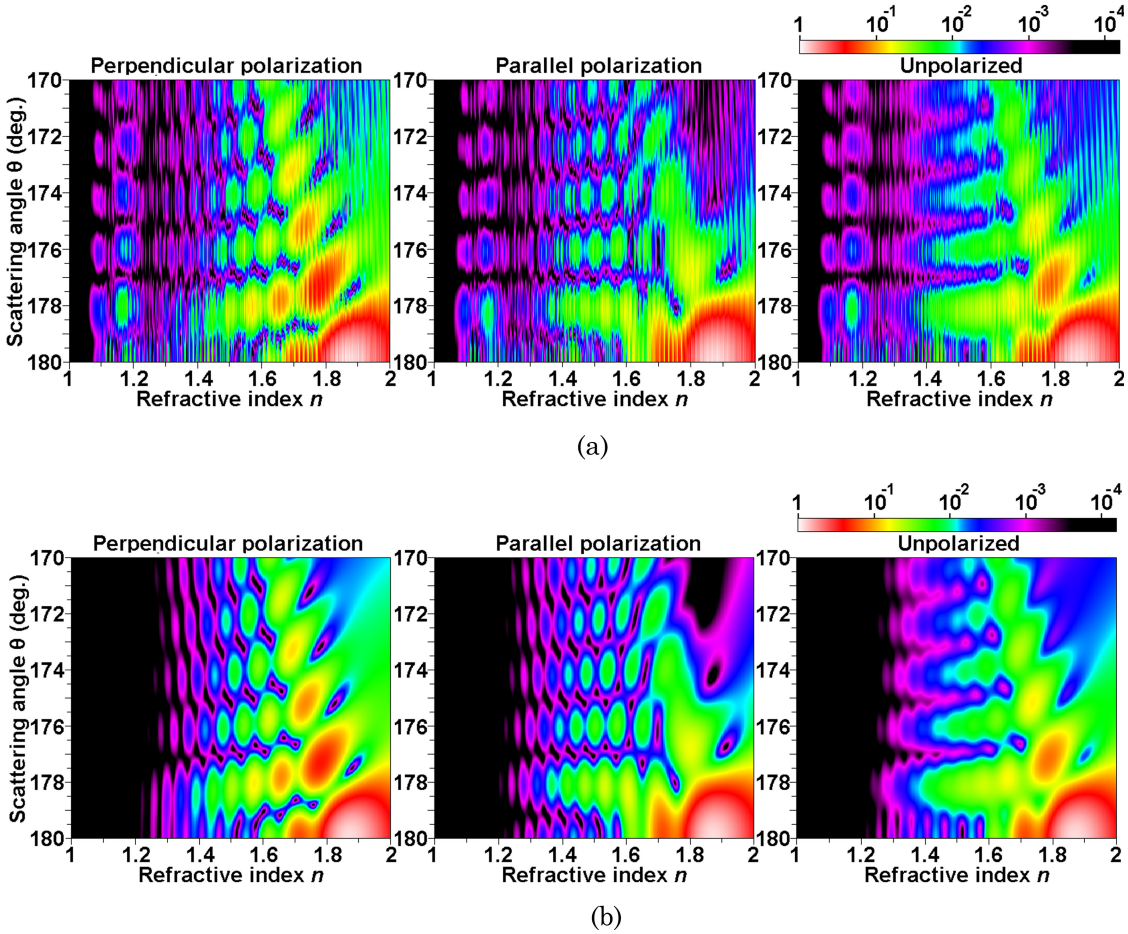

Fig. 2. (Color online) False-color maps showing the intensity of scattering of red light ($\lambda = 650\,\text{nm}$) by a sphere of radius $r = 10\,\mu\text{m}$ for scattering angle $\theta = 170° - 180°$ as a function of refractive index n of the sphere using (a) Mie calculations and (b) Debye series $p = 2$ calculations. Left, perpendicular polarization; center, parallel polarization; right, unpolarized.

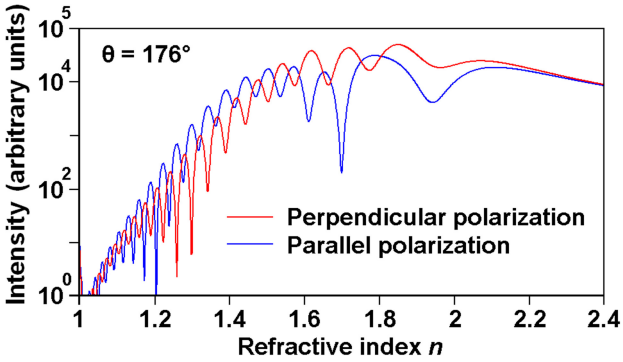

Fig. 3. (Color online) Debye series $p = 2$ calculations of intensity for scattering of red light ($\lambda = 650$ nm) at $\theta = 176°$ by a sphere with radius $r = 10\,\mu$m as a function of n.

these features are roughly horizontal is the first indication that the angular size of the glory's rings might be almost independent of n.

Figure 2(b) is an equivalent false-color map based on results for Debye series calculations [8] for $p = 2$, thus revealing the intensity of scattering caused by rays that have suffered one internal reflection within the scattering sphere. Most of the features of Fig. 2(a) also appear in Fig. 2(b), confirming the dominance of $p = 2$ scattering in backscattering. Despite the strong similarities, Fig. 2(a) shows various features that do not appear in Fig. 2(b), such as the vertical striations caused by resonances, which change very rapidly as a function of n. Another difference is that Fig. 2(a) shows glory rings for $n \approx 1.18$ and $n \approx 1.1$, which are due to $p = 3$ and $p = 4$ scattering, respectively. Note that the rings of these glories occur at values of θ identical to those for the $p = 2$ glory at higher values of n.

The false-color maps in Fig. 2 contain various puzzling features. For example, in Fig. 2(b), unpolarized light at $\theta \approx 176°$ does not exhibit strong maxima or minima as a function of n, yet the maxima for perpendicular polarization as a function of n seem to coincide with the minima for parallel polarization (and vice versa). This behavior is shown more clearly in Fig. 3, which also indicates that parallel polarization tends to be dominant when $n < 1.5$. Note that Fig. 3 shows that the intensity of $p = 2$ scattering at $\theta = 176°$ decreases rapidly as n is reduced below $n \approx 1.5$: for example, the intensity when $n = 1.2$ is about 1% of the intensity when $n = 1.5$. More generally, the maps in Fig. 2(b) show horizontal bands of higher intensity at specific values of θ: these horizontal bands indicate that the rings of glories appear at values of θ that seem to be almost independent of refractive index n.

In 1947, van de Hulst [9] postulated that surface waves play a crucial role in the formation of glories when $n < \sqrt{2} \approx 1.41$. However, glories can be formed by geometric rays without the need for surface waves when $n > 1.41$. Consequently, one might have expected to see some discontinuity or transition in

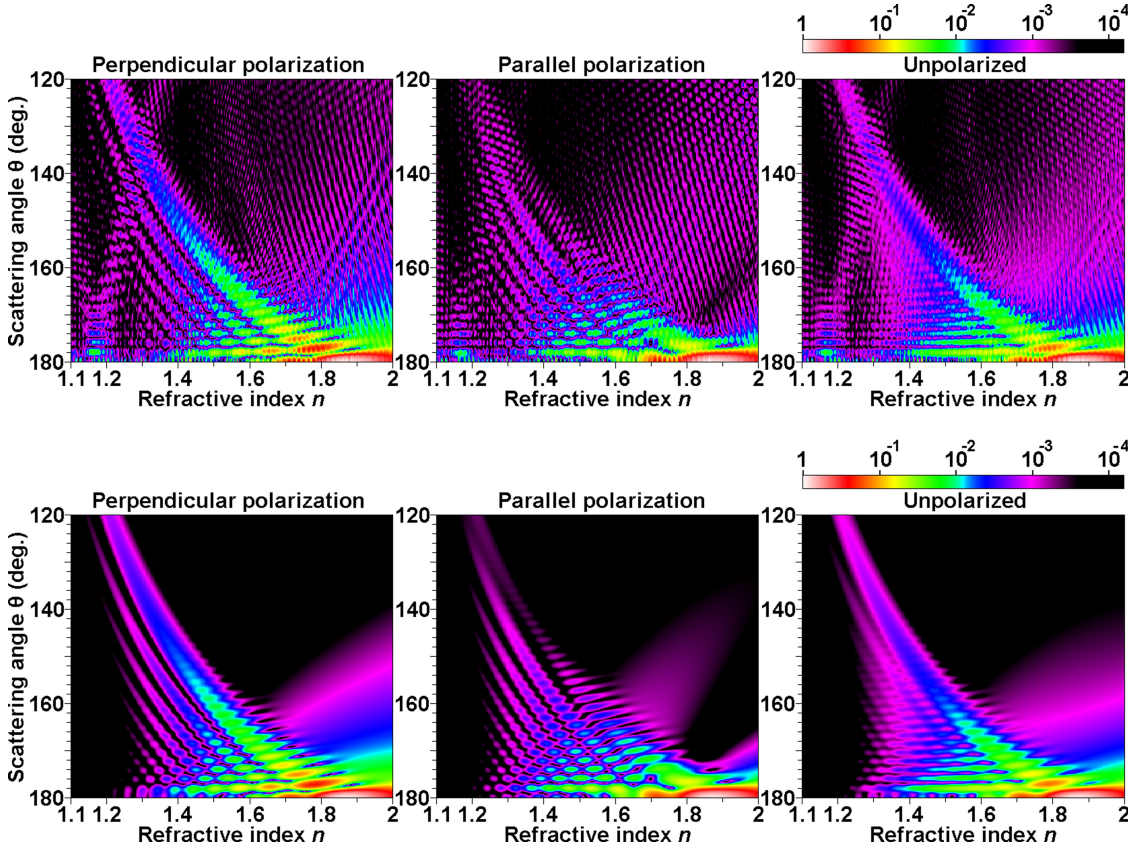

Fig. 4. (Color online) As Fig. 2 but for $\theta = 120°$–$180°$ using (a) Mie calculations and (b) Debye series $p = 2$ calculations.

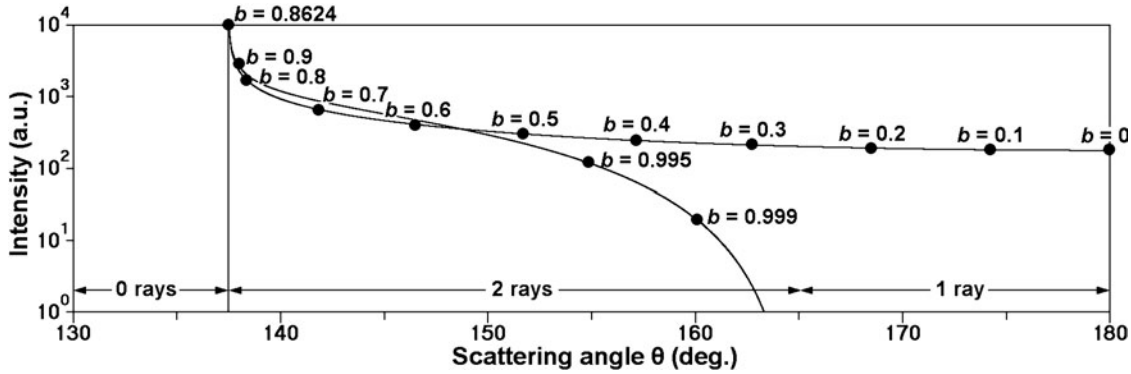

Fig. 5. Results of ray tracing calculations showing the intensity of $p = 2$ scattering of red light ($\lambda = 650\,\text{nm}$) by a sphere of radius $r = 10\,\mu\text{m}$ as a function of scattering angle θ (for perpendicular polarization) for $n = 1.33$. The curves are marked with the impact parameter b, where $b = 0$ is a central ray and $b = 1$ is an edge ray. Rays with $b = b_r \approx 0.8624$ cause scattering at the rainbow angle of 137.5°, while $b = 1$ corresponds to $\theta = 165°$. Type A rays are defined by $0 < b < b_r$, while type B rays are defined by $b_r < b < 1$. There are no geometric $p = 2$ rays when $\theta < 137.5°$, two rays when $137.5° < \theta < 165°$, and one ray when $165° < \theta < 180°$.

the false-color maps around $n = 1.41$ corresponding to the change in mechanisms for production of the glory. Why is there is no sign of such a transition in Fig. 2?

To gain a better understanding of the backscattering processes, it is useful to extend the false-color maps to cover a wider range of scattering angles—such as those in Fig. 4 for $120° \le \theta \le 180°$. Figure 4(a) shows the results of Mie calculations, while Fig. 4(b) shows the results of Debye $p = 2$ calculations. These maps confirm the importance of $p = 2$ scattering over the wider range of θ. Figure 4(a) is heavily dappled, but the dappling in Fig. 4(b) has a surprisingly regular pattern of maxima and minima. Again, at specific values of θ corresponding to the rings of the glory, the maxima for perpendicular polarization as a function of n coincide with minima for parallel polarization (and vice versa).

3. Ray Tracing

Although the false-color maps shown in Fig. 2 and 4 are based on rigorous calculation methods (Mie and Debye), it is helpful to consider the results of approximate calculation methods such as geometric ray tracing. Figure 5 shows the results of ray tracing calculations for $r = 10\,\mu\text{m}$, $p = 2$, and $n = 1.33$. A ray with impact parameter $b = 0$ (i.e., a central ray) results in a scattering angle $\theta = 180°$. As b increases, θ is reduced until $b = b_r = 0.8624$ when θ reaches its minimum value at $\theta = 137.5°$ (the primary rainbow angle), where ray tracing calculations wrongly show a sharp spike of intensity. As b is increased further, θ increases until $\theta = 165°$, when $b = 1$ (corresponding to an edge ray). No geometric $p = 2$ rays can produce scattering when $\theta < 137.5°$, but two such rays can cause scattering when $137.5° < \theta < 165°$: for example, Fig. 6 shows that scattering at $\theta = 141°$ can be caused by a ray with $b = 0.7201$ and by another ray with $b = 0.9477$. As an aid to understanding the false-color maps in this paper, it is useful to designate rays with $0 < b < b_r$ as type A rays and those with $b_r < b < 1$ as type B rays. Figure 5 shows that the intensities due to these type A and type B rays are similar when $\theta < 150°$. As the path lengths of the type A and type B rays are slightly different for a given value of θ, the resulting interference pattern corresponds to the supernumerary arcs of the primary rainbow. Note that because only one geometric $p = 2$ ray can contribute to scattering when $165° < \theta < 180°$, ray tracing is unable to predict the glory for $n = 1.33$. (When $n < 1.41$, the glory is caused by surface waves triggered by rays with impact parameter $b = \pm 1$.)

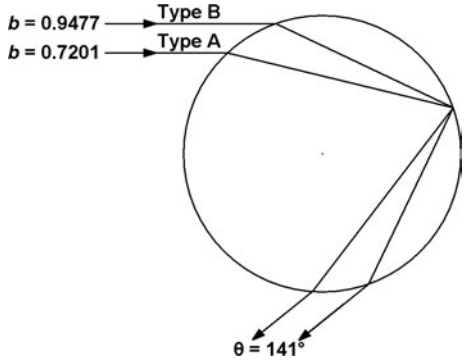

Fig. 6. Paths of geometric $p = 2$ rays resulting in $\theta = 141°$ for $n = 1.33$.

Figure 7 shows that the situation is very different when $n = 1.8$. Although $b = 0$ again results in $\theta = 180°$, the primary rainbow occurs at $\theta = 175.5°$ when $b = b_r = 0.5033$. As b is increased further, θ reaches 180° when $b = b_{180} = 0.785$. Further increases in b cause the deviation D of the incident ray to exceed 180°. Because of spherical symmetry, if $180° < D < 360°$, this is equivalent to scattering angle $\theta = 360° - D$. More generally, scattering at angle $\theta = 180° - \delta$ (where $0 < \delta < 180°$) could be the result of light being deviated by $180° - \delta$ or $180° + \delta$. When $n = 1.8$, only one geometric ray contributes to scattering when $135° > \theta < 175.5°$, while three geometric rays contribute when $175.5° < \theta < 180°$. The ray tracing diagram in Fig. 8 for $n = 1.8$ shows an example of how three geometric rays contribute to scattering at $\theta = 176°$. To take account of deviations greater than

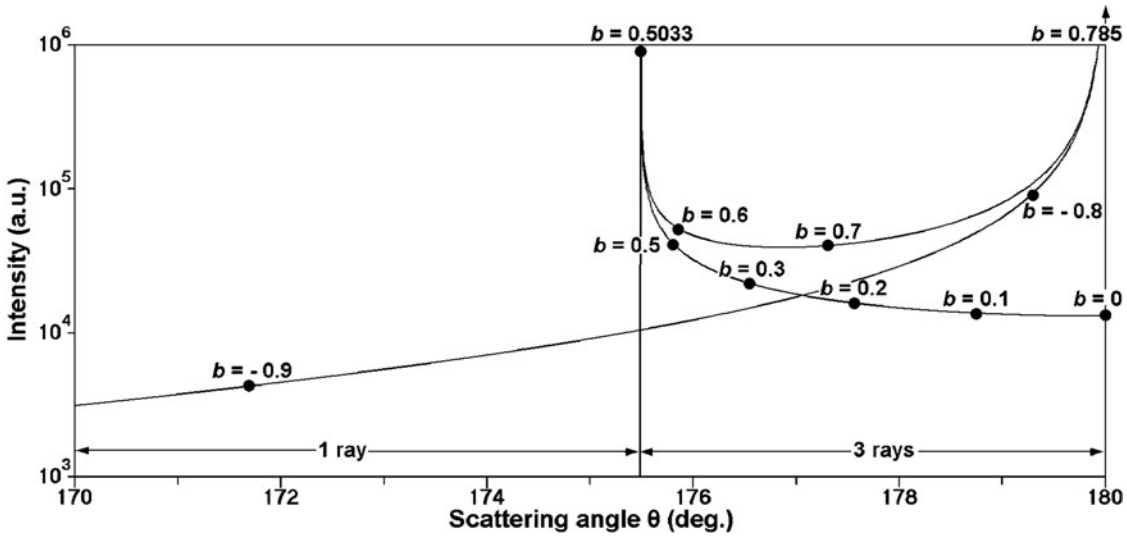

Fig. 7. As in Fig. 5 except that $n = 1.8$. Rays with $b = b_r \approx 0.5033$ cause scattering at the rainbow angle of 175.5°, while $b = b_{180} \approx 0.785$ corresponds to $\theta = 180°$. Type A rays are defined by $0 < b < b_r$, while type B rays are defined by $b_r < b < b_{180}$, and type C rays are defined by $-b_{180} > b > -1$. There is one geometric $p = 2$ ray when $135° < \theta < 175.5°$ and three rays when $175.5° < \theta < 180°$.

180° that occur when $n > 1.41$, type B rays must be redefined as $b_r < b < b_{180}$ together with the addition of type C rays, which are defined by $-b_{180} > b > -1$ (e.g., $-0.785 > b > -1$ for $n = 1.8$). Note that the type C ray in Fig. 8 causes a deviation of 184°, which is equivalent to $\theta = 360° - 184° = 176°$.

It is relatively simple to determine the number of geometric rays that contribute to scattering at specific values of θ and n, as illustrated in Fig. 9. The boundaries between the zones in Fig. 9 correspond to the geometric rainbow angle (at which there is a transition between two rays and no rays, or a transition between three rays and one ray) and to the value of θ corresponding to edge rays ($b = \pm 1$). Note that the zone with three rays covers a substantial range of values of θ and n. As we will see shortly, this three-ray zone is particularly important for the formation of glories when $n > 1.41$.

Figure 10 contains a set of false-color maps for $p = 2$ scattering based on ray tracing calculations. Figure 10(a) shows the intensity of contributions made by type A rays, while Fig. 10(b) shows the intensity of contributions made by type B rays. In both cases, it is easy to see that the upper boundary of the contributions is defined by a distinct curve—in fact, this curve corresponds to the geometric rainbow angle shown by the dashed curve in Fig. 9. The vector sum of the contributions from type A and type B rays is shown in Fig. 10(c). Interference between type A and type B rays results in the supernumerary arcs of the primary rainbow. Note that the maxima of the supernumerary arcs for perpendicular polarization coincide with the minima of the supernumerary arcs for parallel polarization [10]. This phenomenon is caused by the fact that, in general, type B rays have an angle of incidence greater than Brewster's angle and, hence, light that is polarized parallel to the scattering plane suffers an additional phase

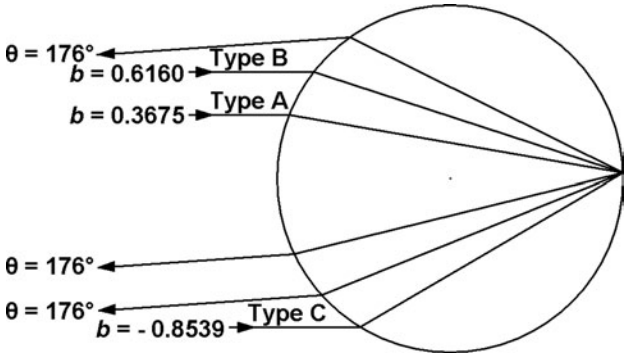

Fig. 8. Paths of geometric $p = 2$ rays resulting in $\theta = 176°$ for $n = 1.8$. Note that the type C ray at $b = -0.8539$ is deviated by 184°, which is equivalent to $\theta = 360° - 184° = 176°$.

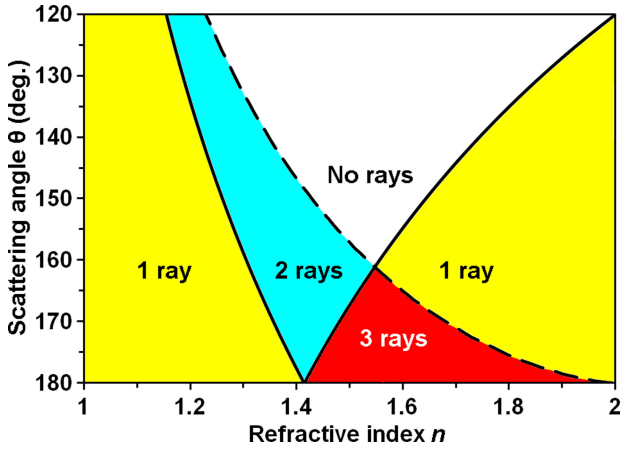

Fig. 9. (Color online) Map of θ and n showing areas where different numbers of geometric $p = 2$ rays contribute to scattering: for example, three geometric rays contribute to scattering at $\theta = 176°$ for $n = 1.8$ (as shown in Fig. 8). The boundaries between these areas are defined by (a) the dashed curve, which shows the variation of the primary rainbow angle as a function of n, and (b) the solid curves, which show the value of θ as a function of n caused by an edge ray (i.e., $b = 1$).

change of 180°. Consequently, the maxima for parallel polarization occur midway between the maxima for perpendicular polarization. Although the supernumerary arcs are just discernible in the right panel of Fig. 10(c) for unpolarized light, viewing the primary rainbow (even with $r = 10\,\mu$m) through a linear polarizing filter will help to reveal the supernumerary arcs.

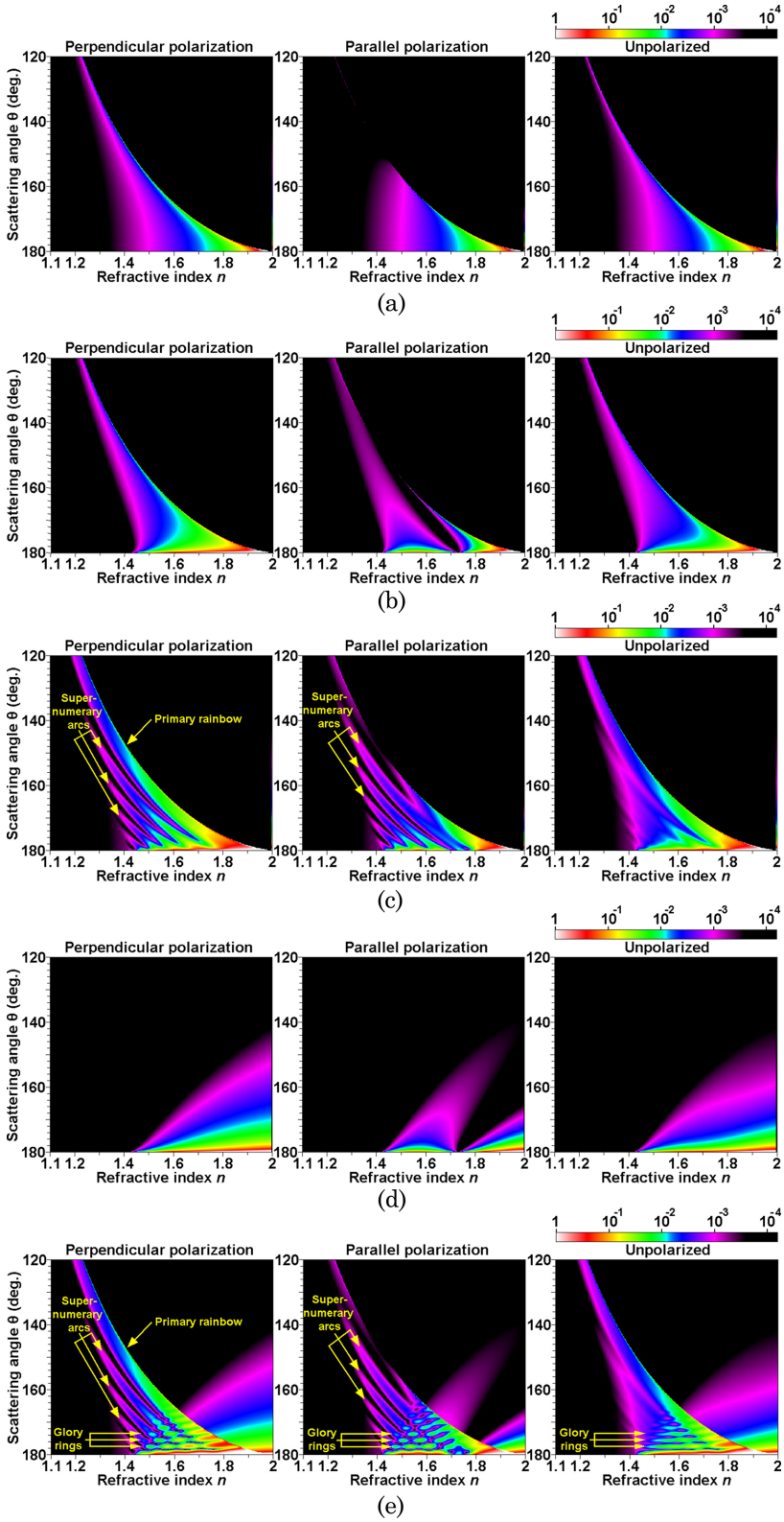

Fig. 10. (Color online) As in Fig. 4, but using $p = 2$ ray tracing calculations: (a) type A rays, (b) type B rays, (c) vector sum of type A and B rays, (d) type C rays, (e) vector sum of type A, B, and C rays.

Figure 10(d) shows the contributions made by type C rays, which occur only when $n > 1.41$. Figure 10(e) shows the vector sum of type A, B, and C rays: the resulting interference patterns include the supernumerary arcs of the primary rainbow [as shown in Fig. 10(c)] together with the rings of the glory. Note the strong resemblance between the ray tracing calculations in Fig. 10(e) and the Debye series calculations in Fig. 4(b): both false-color maps show the appearance of the glory rings at values of θ that are independent of n. Furthermore, both maps show the same form of regular dappled pattern of maxima and minima in the zone marked "3 rays" in Fig. 9. It seems that this pattern is due to the superimposition of the diagonal maxima and minima of the supernumerary arcs onto the horizontal maxima and minima of the glory rings.

4. Surface Waves

One key difference between Fig. 4(b) and Fig. 10(e) is that the latter shows limited backscattering when $n < 1.41$, especially in the zone marked "1 ray" on the left side of Fig. 9. In this zone, it is important to consider the role of surface waves—which are generated by edge rays (i.e., incident light with impact parameter $b = \pm 1$). Unfortunately, there are no

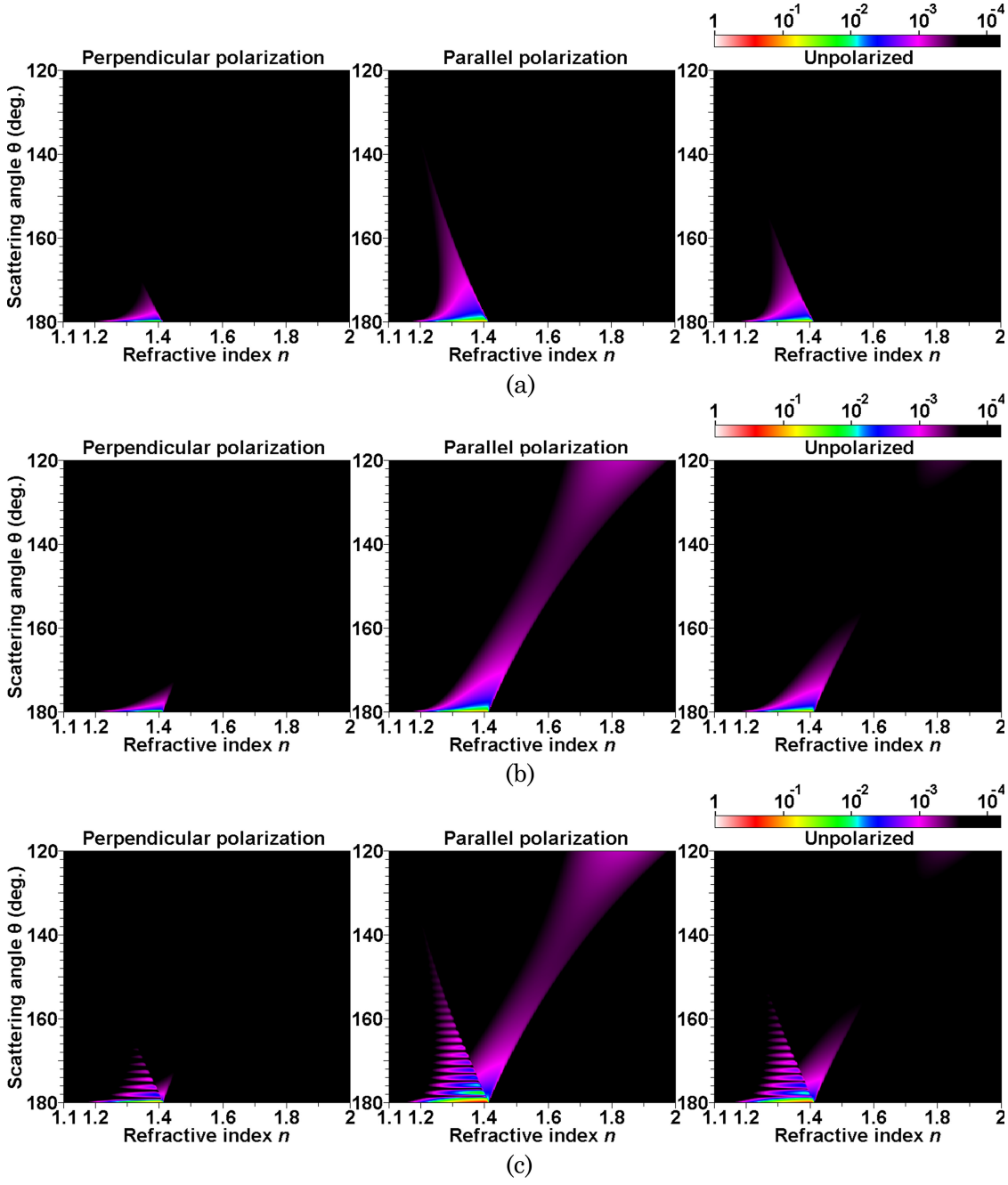

Fig. 11. (Color online) As in Fig. 4, but using $p = 2$ surface wave calculations: (a) short-path contributions (i.e., deviation < 180°), (b) long-path contributions (i.e., deviation > 180°), (c) vector sum of short-path and long-path contributions.

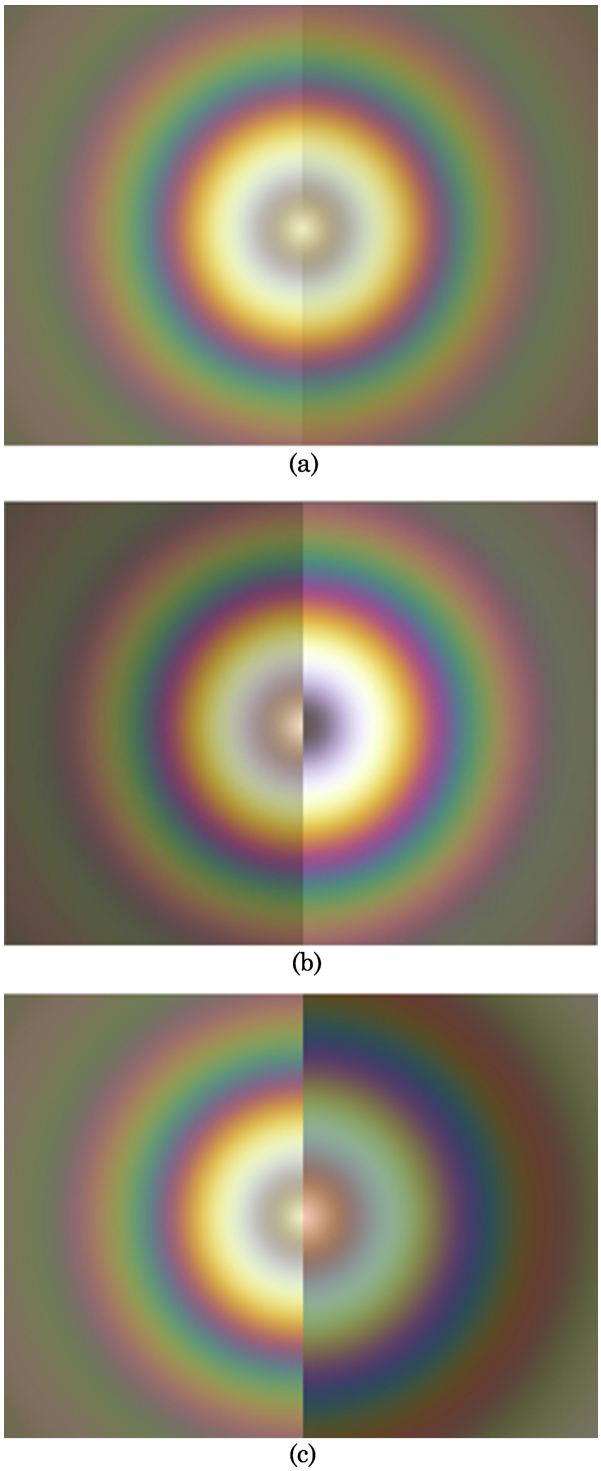

Fig. 12. (Color online) Full-color simulations of a glory caused by scattering of sunlight by spherical droplets of radius $r = 10\,\mu$m. (a) Left, water (n varies with wavelength); right, fixed value of $n = 1.3333$. (b) Left, fixed value of $n = 1.2$; right, fixed value of $n = 1.5$. (c) Left, water (n varies with wavelength); right: fixed value of $n = 1.7$.

rigorous methods for calculation of scattering by surface waves. The calculations reported in this section are based on the approximation provided by Khare [11] modified by an amplitude correction factor of 0.5 used in previous work [12] for $p = 2$ surface waves.

As mentioned above, scattering in a specific direction such as $\theta = 180° - \delta$ can be considered as the vector sum of light that has been deviated by $180° - \delta$ (known as "short-path" contributions, which are similar to type B rays) and of light that has been deviated by $180° + \delta$ (known as "long-path" contributions, which are similar to type C rays). The false-color map in Fig. 11(a) shows the surface wave contributions to scattering due to light that has been deviated by less than 180° ("short path"), while Fig. 11(b) shows the surface wave contributions involving deviations of more than 180° ("long path"). The center panels show the strongest scattering because surface waves are predominantly polarized parallel to the scattering plane. Figure 11(c) shows the vector sum of the contributions in Figs. 11(a) and 11(b). Interference between the short-path and long-path contributions results in a series of maxima at $\theta = 180°$, $\theta \approx 178°$, $\theta \approx 176°$, and so on. Obviously, these maxima represent the rings of the monochromatic glory. Previous work [12] indicated that the approximate calculation methods for the intensity of surface waves do not give accurate results for the phase of the surface wave contribution—and, hence, the location of the maxima would also be inaccurate. Even so, the fact that these maxima appear as horizontal features in Fig. 11(c) provides further confirmation that the angular size of the glory rings is not dependent on the refractive index n of the sphere.

The short path corresponding to a deviation of $180° - \delta$ and the long path corresponding to a deviation of $180° + \delta$ differ in physical path length (see Fig. 7 of [12]). The extra length traveled by the long-path surface wave along the circumference of the sphere is equivalent to the length of the arc subtended by the angle 2δ. If δ is measured in degrees, this difference in physical path length is $2\pi r(2\delta/360°) = \pi r\delta/90°$. The speed of propagation of surface waves is determined by the refractive index n_{med} of the medium in which the sphere is immersed (rather than the refractive index n of the sphere). Consequently, the interference pattern due to the short-path and long-path surface waves should exhibit maxima when $\pi r(\delta/90°)/n_{\text{med}} = m\lambda$, where m is a positive integer. In the case under study ($r = 10\,\mu$m, $\lambda = 0.65\,\mu$m, and $n_{\text{med}} = 1$), the resulting maxima should be at intervals of 1.86° from 180° (i.e., at $\theta = 180°$, $\theta \approx 178.1°$, $\theta \approx 176.3°$, $\theta \approx 174.4°$, etc.). This simplistic treatment gives values similar to those found elsewhere in this paper by using rigorous calculation methods (Mie and Debye).

5. Full-Color Simulations of Glories

All of this paper's calculations have so far assumed a monochromatic light source ($\lambda = 650$ nm). Of course, we are much more interested by glories caused by scattering of a continuous spectrum (e.g., sunlight). The left-hand side of Fig. 12(a) shows a simulation of the glory caused by scattering of sunlight by water

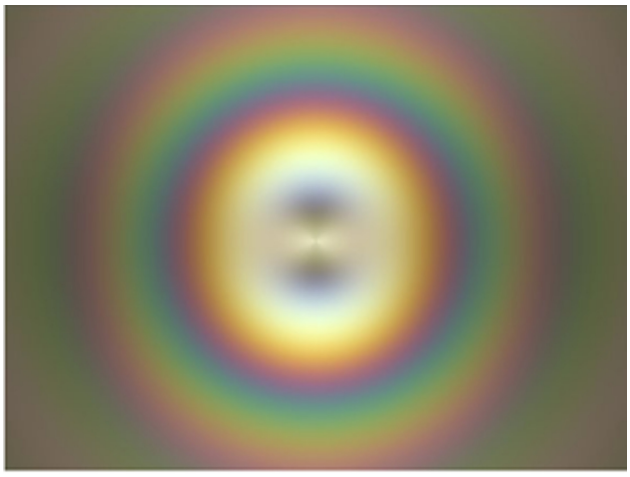

(a)

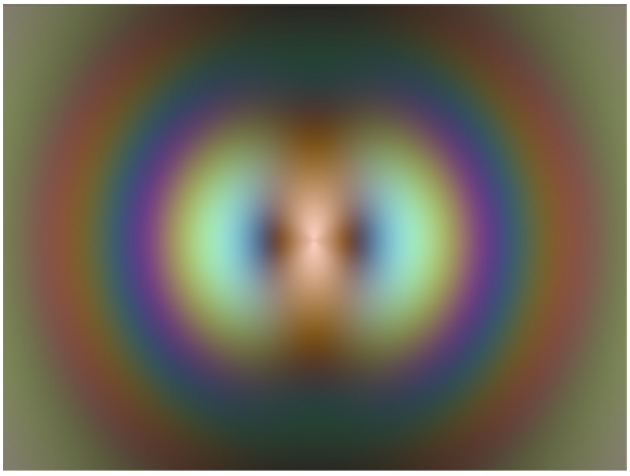

(b)

Fig. 13. (Color online) Full-color simulations of a glory caused by scattering of sunlight by spherical droplets of radius $r = 10\,\mu$m as viewed through a vertical polarizer: (a) water (n varies with wavelength); (b) fixed value of $n = 1.7$.

droplets of radius $r = 10\,\mu$m (with n varying between 1.3445 at $\lambda = 400$ nm and 1.3314 at $\lambda = 700$ nm). The right-hand side of Fig. 12(a) shows the glory resulting from the same conditions except that $n = 1.3333$ across the visible spectrum. The strong similarity between these simulations indicates that, unlike the rainbow, the colors of the glory are NOT caused by the variations in n across the visible spectrum.

The simulations shown in Fig. 12(b) compare the glory caused by droplets with fixed value of $n = 1.2$ with the glory caused by droplets with fixed value of $n = 1.5$. Figure 12(c) compares the glory caused by water droplets (with n varying between 1.3445 at $\lambda = 400$ nm and 1.3314 at $\lambda = 700$ nm) with the glory caused by droplets with fixed $n = 1.7$. Even with this large disparity in refractive index, there are only minor changes in the appearance of the glory.

When $n < 1.41$, glories are caused by surface waves—which are polarized parallel to the scattering plane. However, when $n > 1.41$, glories are caused by geometric rays in the vicinity of the primary rainbow—and are thus dominated by perpendicular polarization. An example of this change in polarization is highlighted by the dramatic differences in full-color simulations of a glory as viewed through a vertical polarizer: Fig. 13(a) shows scattering from water droplets, while Fig. 13(b) shows scattering from droplets with a fixed value of $n = 1.7$. Further studies are needed to establish whether viewing glories through polarizing filters could give a rough indication of the value of n.

Figure 14 shows full-color simulations (using Mie calculations) of scattering of sunlight from a spherical droplet with $r = 10\,\mu$m to illustrate variations in the colors of the glory as a function of refractive index n. Figure 14 indicates that, when $1.03 < n < 1.7$, the angular size of the glory's rings (and the colors of the rings) are, to a large degree, independent of n.

6. Conclusions

Glories are the result of backscattering of light from spherical droplets. It is surprising to find that the size of a glory's rings (and the colors of the rings) are almost independent of the refractive index n of the droplet—at least for $1.03 < n < 1.7$. One explanation for this behavior is that surface waves (which are crucial for the formation of glories when $n < 1.41$) propagate at a speed determined by the refractive index n_{med} of the medium rather than n. As the glory's rings are caused by interference between counterrotating surface waves, the interference pattern is determined

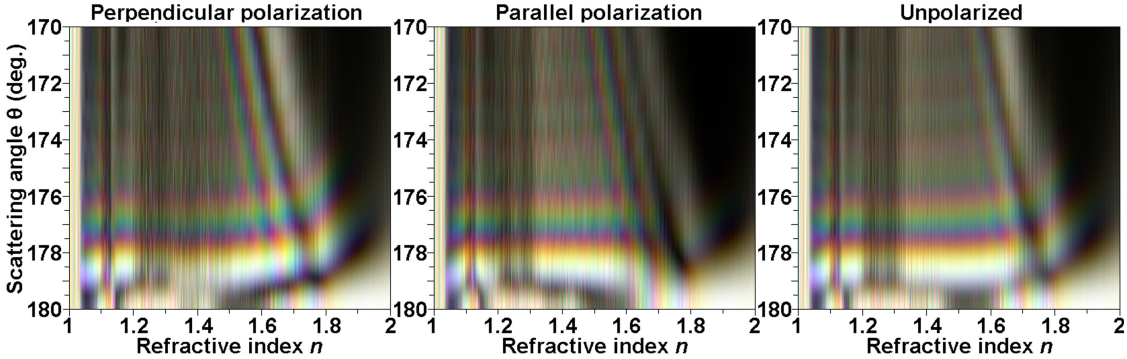

Fig. 14. (Color online) Colors of the glory caused by scattering of sunlight by spherical water droplets of radius $r = 10\,\mu$m as a function of refractive index n (assuming a fixed value of n across the visible spectrum).

by the radius r of the droplet, the wavelength λ of the illuminating light, and the refractive index n_{med} of the medium—and not by the refractive index n of the droplet.

Full-color simulations of glories confirm that the colored rings of glories have a very consistent appearance even for wide variations in n. This finding suggests that observations of glories can yield useful information about the value of r, but little information about the value of n. Further work is needed to establish whether viewing glories through polarizing filters could provide a rough indication of the value of n.

References

1. J. E. Hansen and J. W. Hovenier, "Interpretation of the polarization of Venus," J. Atmos. Sci. **31**, 1137–1160 (1974).
2. G. P. Können, "A halo on Mars," Weather **61**, 171–172 (2006).
3. P. Laven, "Atmospheric glories: simulations and observations," Appl. Opt. **44**, 5667–5674 (2005).
4. C. A. Griffith, P. Penteado, P. Rannou, R. Brown, V. Boudon, K. H. Baines, R. Clark, P. Drossart, B. Buratti, P. Nicholson, C. P. McKay, A. Coustenis, A. Negrao, and R. Jaumann, "Evidence for a polar ethane cloud on Titan," Science **313**, 1620–1622 (2006).
5. S. D. Gedzelman, "Simulating glories and cloudbows in color," Appl. Opt. **42**, 429–435 (2003).
6. P. Laven, "Simulation of rainbows, coronas, and glories by use of Mie theory," Appl. Opt. **42**, 436–444 (2003).
7. L. Cowley, IRIS software available at http://www.atoptics.co.uk/droplets/iris.htm.
8. E. A. Hovenac and J. A. Lock, "Assessing the contributions of surface waves and complex rays to far-field Mie scattering by use of the Debye series," J. Opt. Soc. Am. A **9**, 781–795 (1992).
9. H. C. van de Hulst, "A theory of the anti-coronae," J. Opt. Soc. Am. **37**, 16–22 (1947).
10. G. P. Können and J. H. de Boer, "Polarized rainbow," Appl. Opt. **18**, 1961–1965 (1979).
11. V. Khare, "Short-wavelength scattering of electromagnetic waves by a homogeneous dielectric sphere," Ph.D. dissertation (University of Rochester, 1976); the calculation method is summarized in [8].
12. P. Laven, "How are glories formed?," Appl. Opt. **44**, 5675–5683 (2005).